Proceedings of the Thirty-second (2022) International Ocean and Polar Engineering Conference **www.isope.org**
Shanghai, China, June 5–10, 2022
Copyright © 2022 by the International Society of Offshore and Polar Engineers (ISOPE)
ISBN 978-1-880653-81-4; ISSN 1098-6189

Numerical Study of Cavitation Noise around 2-D Hydrofoil with Direct Volume Integration

*Lianjie Yu[1], Qingjie Meng[2], Decheng Wan[1]**

[1] Computational Marine Hydrodynamics Lab (CMHL), School of Naval Architecture, Ocean and Civil Engineering, Shanghai Jiao Tong University, Shanghai, China
[2] Wuhan Second Ship Design and Research Institute, Wuhan, China
*Corresponding author

ABSTRACT

Underwater noise (URN) is the focus of academic research, and cavitation is an important source of underwater noise. This paper takes NACA66 (mod) two-dimensional hydrofoil as the research object, and uses the open source software OpenFOAM to simulate the sheet cavitation and sound field. The turbulence model is DDES, and the cavitation model is the Schnerr-Sauer model. The sound field is predicted by the FW-H formulation. Unlike the traditional method, this paper solves the quadrupole term (non-linear term) by direct volume integration, so the nonlinear term can be predicted more accurately. At the same time, a new method of changing sound wave velocity is proposed considering the two-phase medium problem caused by cavitation. Four methods are compared including two-phase volume integration, direct volume fraction, object surface integration and penetrable formulation. It was found that the influence of two-phase flow is greater near the closure area of the cavity, which needs to be considered separately. The closer to the cavity closure zone, the greater the nonlinear effect.

KEY WORDS: cavitation noise, NACA66 (mod), FW-H formulation, direct volume integration.

INTRODUCTION

The underwater noise not only causes harm to marine life, but also affects the stealth of military equipment. The International Maritime Organization (IMO) issued non-mandatory noise standards for commercial ships (IMO, 2014). More and more attention is paid to the acoustic environment. At this stage, the prediction of such noise becomes a hot topic (Deane, 2010; Ianniello, 2013; Bensow, 2016).

The underwater noise can be divided into three parts: structure vibration noise, propeller noise and flow-induced noise. Flow-induced noise is caused by pressure fluctuations. As the speed of structures increases, the impact of flow-induced noise also increases. Theoretically, prediction of the flow-induced noise needs to directly solve the compressible N-S equation, but the solution strategy in aerodynamics cannot be applied to the water medium, and this method is computationally expensive (Cianferra, 2019). In recent years, acoustic analogy has been adopted in most researches (Epikhin, 2015; Schmalz, 2015; Choi, 2016). Within this framework, the flow field is regarded as the sound source, and the free space Green's function is used to describe the sound pressure propagation in the far field. The acoustic analogy was first proposed by Lighthill (1952) and developed by Curle (1955), Ffowcs Williams (1969) and others. By now, it has achieved great development. The commonly-used formulation is called FW-H equation, which regards the various motion of solid objects as sound sources.

The FW-H equation was first proposed in the aerodynamics. The equation contains 3 kinds of sound sources: monopole, dipole and quadrupole. The monopole sound source is caused by the movement of the object. The dipole is caused by the pressure fluctuation near the object. And the quadrupole sound source is caused by the turbulent behavior of the flow itself (such as vortex, shock wave, etc.). The quadrupole term (nonlinear sound source) has little effect on noise in the air, and it requires expensive volume integrations, so this term is often ignored. However, the results of hydrodynamic noise in recent years showed that the influence of the quadrupole is important, even dominates the acoustic far field (Choi, 2016; Cianferra, 2018). Therefore, the quadrupole term must be considered for the prediction of underwater noise.

An alternative choice is the penetrable FW-H formulation, which moves the integral surface from the object to the flow field. Such integration is believed to consider the nonlinear terms enclosed by the porous surface. However, this approach is greatly affected by the selection of the penetrable surface (Cianferra, 2019). The direct volume integration is the most accurate way to calculate the quadrupole. Some scholars carried out the volume integration successfully (Cianferra, 2018; Cianferra, 2019). It is found that the computation cost is within an acceptable range, if the time delay is ignored (compact source hypothesis). And the requirements of compact sound sources are met for most of the underwater flows (low Mach number).

As far as the author knows, there is no application of direct volume integration to the cavitation noise problems. Cavitation is the most significant cause of underwater noise (Ahn, 2016; Wu, 2018; Sun, 2020). It is necessary to study the nonlinear term of cavitation noise. Hydrofoil is a typical geometry for study of cavitation, and many scholars conducted in-depth research on it (Kim, 2017; Kim 2018; He, 2020). Among them, the NACA66 series are mostly used, for the abundant experimental and simulation data (Singhal, 2002; Wang, 2021).

This paper takes NACA66 (MOD) model as the research object. The noise characteristics of hydrofoil cavitation is analyzed from the perspectives of sound source distribution, near-field sound pressure, far-field attenuation law, acoustic directivity, etc. The research is hoped to contribute to the understanding of cavitation noise.

THE MATHEMATICAL FORMULATIONS

Turbulence model

The problem of cavitation is still an open issue, and the interaction between turbulence and cavitation is particularly complex. Previous studies proved that the RANS model cannot obtain the small-scale vortices in the cavitation flow, which has a great impact on the acoustic prediction.

For this reason, this paper uses the improved Spalart-Allmaras DES as the turbulence model, namely SA-DDES (Spalart, 1992). Its governing equation is,

$$\frac{\partial \tilde{v}}{\partial t} + div(\tilde{v}u) = \frac{1}{C_\sigma}\{div[(v+\tilde{v})grad\tilde{v}] + C_{b2}\frac{\partial \tilde{v}}{\partial x_i}\frac{\partial \tilde{v}}{\partial x_j}\} + C_{b1}\tilde{S}\tilde{v} - C_{w1}f_w(\frac{\tilde{v}}{\tilde{d}})^2 \quad (1)$$

The first term on the left side is the transient term, and the second term is the convection term; the first term on the right side is the diffusion term, the second term is the source term, and the third term is the dissipation term. The DDES equation modifies $\tilde{d}$ in the formula to

$$\tilde{d} = d_w - f_d \cdot \max(d_w - C_{DES}\Delta, 0) \quad (2)$$

$$f_d = 1 - \tanh[(8r_d)^3] \quad (3)$$

$$r_d = \frac{v_t + v}{\sqrt{U_{ij}U_{ij}}(\kappa d_w)^2} \quad (4)$$

Original FW-H formulation

In this paper, the acoustic analogy is used to calculate the far-field noise. The basic equation of acoustic analogy—Lighthill equation is derived on the basis of the N-S equation. Since no assumptions were introduced in the derivation process, it is considered to be the most potential noise computation method. The Lighthill equation can be written as:

$$\frac{\partial^2 \rho'}{\partial t^2} - c_\infty^2 \frac{\partial^2 \rho'}{\partial x_i^2} = \frac{\partial^2 T_{ij}}{\partial x_i \partial x_j} \quad (5)$$

In the formula, $i, j = 1,2,3$. t represents time. ρ' is density fluctuation. c_∞ is the speed of sound in a homogeneous medium, which is 340m/s in air. x_i represents the displacement in the i degree of freedom. T_{ij} is the Lighthill tensor, and the specific form is:

$$T_{ij} = \rho v_i v_j - [(p - p_\infty) - (\rho - \rho_\infty)c_\infty^2]\delta_{ij} - \sigma_{ij} \quad (6)$$

After decades of development, the Lighthill equation continues to evolve. According to the different motion forms, different source terms need to be introduced to the right side of the wave equation to produce different equation forms. Among them, the most widely used and universally significant is the Ffowcs Williams and Hawkings (FW-H) equation, which considers three types of sources: monopole, dipole and quadrupole. After deduction, the FW-H equation based on the Lighthill equation can be written as (Ffowcs, 1969):

$$\left(\frac{1}{c^2}\frac{\partial^2}{\partial t^2} - \nabla^2\right)p' = \frac{\partial}{\partial t}[\rho_0 v_n \delta(f)] - \frac{\partial}{\partial x_i}[p n_i \delta(f)] + \frac{\partial^2}{\partial x_i \partial x_j}[H(f)T_{ij}] \quad (7)$$

The surface of an object can be represented by $f(x,t) = 0$, where $\nabla f = \vec{n}$ points to the normal direction outside the object surface. According to the linear assumption, $p' = c^2\rho' = c^2(\rho - \rho_0)$, where $c$and ρ_0 respectively represent the fluid sound velocity and density under the undisturbed fluid medium. $\delta(f)$ represents the Dirac function, and the corresponding Heaviside unit function is

$$H(f) = \begin{cases} 1, x \in V \\ 0, x \in S \end{cases} \quad (8)$$

The National Aeronautics and Space Administration (NASA) summarized the different integral solutions of the FW-H equation and systematically named these solutions, such as Farassat Formulations 1 and Farassat Formulations 1A. The derivation process of Farassat Formulation 1A is omitted here, and the integral result expression is directly given as follows:

$$4\pi p'_T(x,t) = \int_{f=0}\left[\frac{\rho_0 \dot{v}_n}{r(1-M_r)^2} + \frac{\rho_0 v_n \hat{r}_i \dot{M}_i}{r(1-M_r)^3}\right]_{ret} dS + \int_{f=0}\left[\frac{\rho_0 c v_n (M_r - M^2)}{r^2(1-M_r)^3}\right]_{ret} dS \quad (9)$$

$$4\pi p'_L(x,t) = \int_{f=0}\left[\frac{\dot{p}\cos\theta}{cr(1-M_r)^2} + \frac{\hat{r}_i \dot{M}_i p\cos\theta}{cr(1-M_r)^3}\right]_{ret} dS + \int_{f=0}\left[\frac{p(\cos\theta - M_i n_i)}{r^2(1-M_r)^2} + \frac{(M_r - M^2)p\cos\theta}{r^2(1-M_r)^3}\right]_{ret} dS \quad (10)$$

Here, p'_T stands for thickness noise. p'_L stands for load noise, (x,t) (y,t) are the space-time variables of the observation point and the sound source respectively; $r = |x - y|$ is the norm of the vector radius from the observation point to the sound source; $\hat{r}_i = \frac{(x-y)}{r}$ represents the normalization of the vector radius; $\mathrm{M_r} = \frac{\hat{r}_i v_i}{c}$ is the sound source Mach number in the satellite coordinate system; $1 - M_r$ is called the Doppler factor; $\dot{v}_n = \frac{\partial}{\partial \tau}(v \cdot n)$ represents the derivative of the speed to the sound source time; $\cos\theta = n_i \hat{r}_i$ is the vector path from the observation point to the sound source; $[\ ]_{\mathrm{ret}}$ is retarded time, which represents the satellite coordinates after considering the Doppler effect.

Direct volume integration

Without loss of generality, assuming that the incoming flow is along the $\mathrm{x_1}$ direction, the three-dimensional free space Green's function is written as (Cianferra, 2018):

$$\mathrm{G(x,t;y,\tau)} = \frac{\delta(g)}{4\pi r^*} \quad (11)$$

with $g = \tau - t + \frac{r}{c_0}$. Some parameter expressions in the formula are:

$$r^* = \sqrt{(x_1 - y_1)^2 + \beta^2[(x_2 - y_2)^2 + (x_3 - y_3)^2]} \tag{12}$$

$$r = \frac{-M_0(x_1 - y_1) + r^*}{\beta^2} \tag{13}$$

$$\beta = \sqrt{1 - M_0^2} \tag{14}$$

To obtain the analytic expression of the quadrupole term, it is necessary to deduce the second-order spatial derivative of the Green's function ($\frac{\partial^2}{\partial x_i \partial x_j}\left[\frac{\delta(g)}{r^*}\right]$). According to the derivative formula of the quotient and the chain derivative rule, there is

$$\frac{\partial}{\partial x_i}\left[\frac{\delta(g)}{r^*}\right] = -\frac{\hat{r}_i}{c_0 r^*}\frac{\partial}{\partial t}[\delta(g)] - \frac{\hat{r}_i^*}{r^{*2}}\delta(g) \tag{15}$$

Combining the derivative term simplification and considering the formula, the analytic expression of the quadrupole term under low Mach number is obtained:

$$\frac{\partial^2}{\partial x_i \partial x_j}\left[\frac{\delta(g)}{r}\right] = \frac{1}{c_0^2}\frac{\hat{r}_i\hat{r}_j}{r}\frac{\partial^2}{\partial t^2}[\delta(g)] + \frac{1}{c_0}\left[\frac{3\hat{r}_i\hat{r}_j - \delta_{ij}}{r^2}\right]\frac{\partial}{\partial t}[\delta(g)] + \left[\frac{3\hat{r}_i\hat{r}_j - \delta_{ij}}{r^3}\right]\delta(g) \tag{16}$$

Finally, the volume fraction of this formula can be used to obtain the influence of the nonlinear term.

Cavitation model

The cavitation model, or mass transport model, is derived from the commonly-used Rayleigh-Plesset cavity dynamics equation. The process of condensation and evaporation in cavitation describes the changes in each phase by adding source terms. This paper adopts the Schnerr-Sauer cavitation model (Schnerr, 2001). The mass conversion equation of the model is as follows:

$$\frac{\partial(\rho_v \alpha_v)}{\partial t} + \frac{\partial(\rho_v \alpha_v u_j)}{\partial x_j} = \dot{m}^+ - \dot{m}^- \tag{17}$$

where α_v is the vapor volume fraction, and the source terms $\dot{m}^+$ and $\dot{m}^-$ represent the evaporation and condensation processes, respectively. When the phase change occurs, there is

$$\dot{m}^+ = \frac{\rho_v \rho_l}{\rho}\alpha_v(1 - \alpha_v)\frac{3}{R_b}\sqrt{\frac{2}{3}\frac{\max(p_v - p, 0)}{\rho_l}} \tag{18}$$

$$\dot{m}^- = \frac{\rho_v \rho_l}{\rho}\alpha_v(1 - \alpha_v)\frac{3}{R_b}\sqrt{\frac{2}{3}\frac{\max(p - p_v, 0)}{\rho_l}} \tag{19}$$

Among them, $\dot{m}^+$ represents the evaporation process, and $\dot{m}^-$ represents the condensation process. R_b is the radius of the cavity, and p_v is the saturation vapor pressure at the local temperature. The calculation formula of the cavity radius is:

$$R_b = \left(\frac{\alpha_v}{(1 - \alpha_v)}\frac{3}{4\pi}\frac{1}{N_b}\right)^{\frac{1}{3}} \tag{20}$$

Among them, $N_b = 10^{13} m^{-3}$ is the cavity number density.

NUMERICAL SETUP

Geometric models

In this paper, NACA66 (mod) hydrofoil is selected as the geometric model, the chord length $c = 0.1$ m, the angle of attack (AOA) selected is 4°, the incoming flow velocity $U_0 = 16.8$ m/s, and the cavitation number is 0.84. The calculation parameter settings are shown in Table 1.

The inlet is about 2c from the leading edge, and the outlet is about 4c length from the trailing edge, as figure 1 shows. The inlet is fixed at the incoming velocity U_0 and the outlet has a fixed pressure. In order to simplify the calculation, the y direction (span direction) is set as one grid, that is to say, a two-dimensional example is used for this cavitation research.

Table 1. The basic parameters of the cavitation calculation

Parameters	Value
Profile	NACA66 (mod)
Chord length	0.1 m
AOA (angle of attack)	4 deg
Cavitation number	0.84
Inflow velocity	16.8 m/s

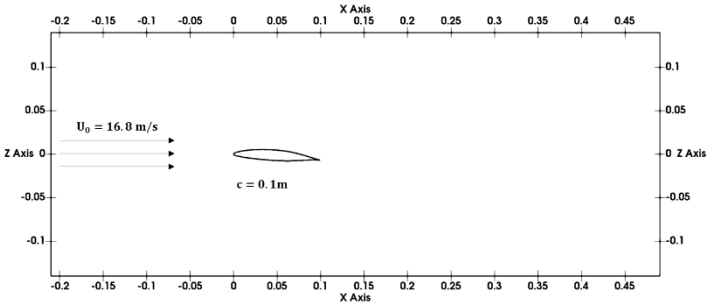

Fig. 1 Computational domain of NACA66 (mod) cavitation domain

Acoustic integration and probes settings

The computational domain is discretized by an unstructured grid, and 5 levels of refinement are set up to capture the cavitation near the hydrofoil, as shown in figure 2.

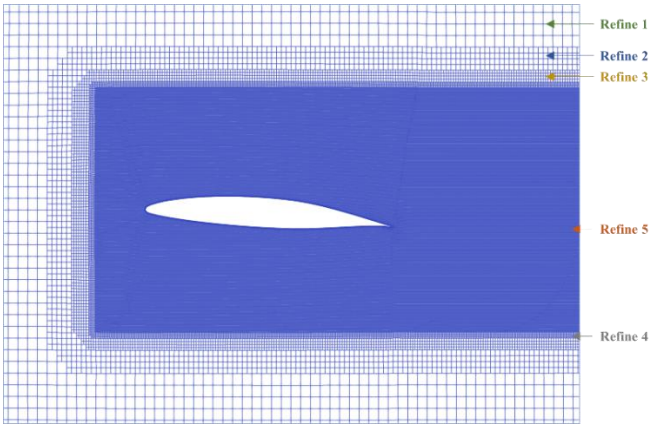

Fig. 2 Unstructured grid with 5 levels of refinement

A volume integration area is selected in the refine 5, and the surface integration is carried out on the hydrofoil. The two kinds of integrals represent the nonlinear term and linear term of sound pressure respectively. To study the near-field acoustic characteristics, 4 probes A, B, C, D are set above the suction surface of the hydrofoil, as shown in the figure 3.

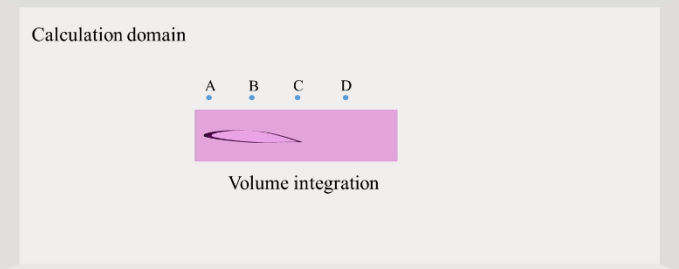

Fig. 3 Volume integration area and acoustic probes

RESULTS AND DISCUSSIONS

Hydrodynamic validation

The working condition in this paper refers to the experiment of Leroux et al. According to the experimental results, when the angle of attack is 4deg and the cavitation number is 0.84, the hydrofoil cavitation is in steady state, showing a sheet shape and hardly break off. The alpha distribution given by the numerical simulation is qualitatively consistent with the experimental results, as shown in the figure 4.

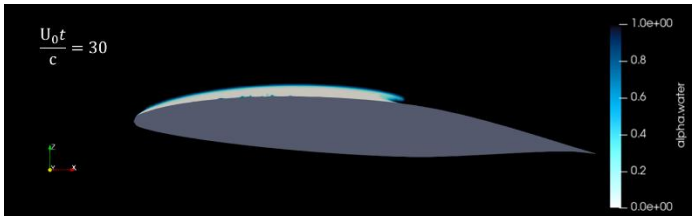

Fig. 4 The sheet cavitation calculated by the numerical simulation.

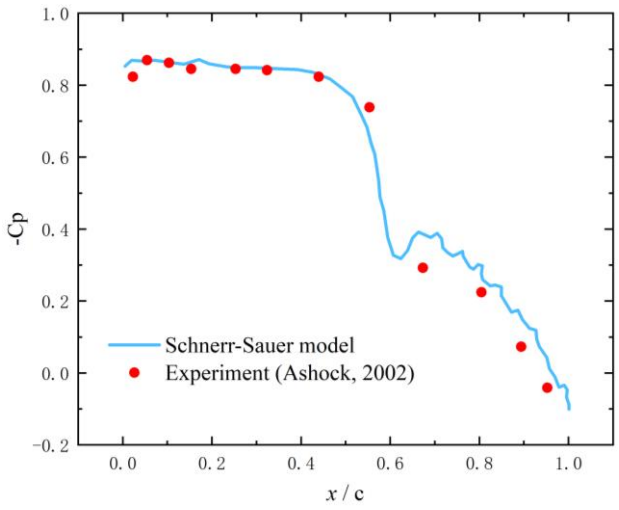

Fig. 5 The pressure coefficient compared with experiment.

The pressure coefficient distribution on the suction surface of the hydrofoil is shown in Figure 5 and compared with the experimental results. When cavitation occurs, the pressure coefficient decreases. It can be seen from the figure 5 that the inverse number of the pressure coefficient decreases at about x/c=0.45 (transition from the cavitation area to the non-cavitation area), and the inflection point of the numerical simulation is about 0.4. Considering the complexity of cavitation flow and the two-dimensional calculation used in this paper, the error is within the allowable range. It can be considered that the flow field results are accurate and reliable, and subsequent acoustic calculations can be performed.

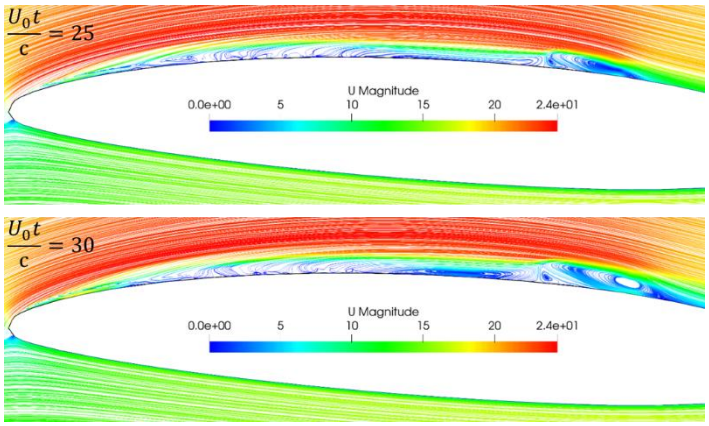

Fig. 6 Stream lines at two moments

Figure 6 shows the two-dimensional streamlines at two moments. It can be seen that a re-entrant jet appears at the bottom of the cavity with the appearance of sheet cavitation, and the re-entrant jet inhibits the further development of the cavity. In many literatures, the re-entrant jet even causes cavitation to shed under high Reynolds number conditions. Such cavitation is called cloud cavitation (Leroux, 2004; Yu, 2021).

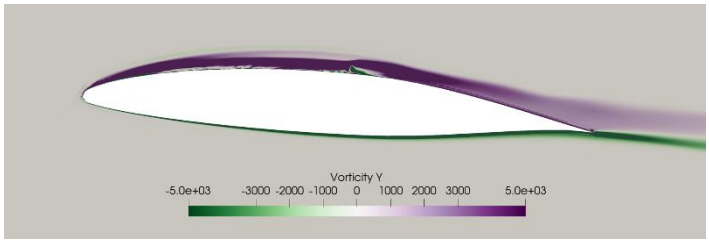

Fig. 7 Contour of ω_Y at moment $\frac{U_0 t}{c} = 30$

The distribution of vortex is related to the non-linear sound sources (quadrupoles). Figure 7 shows the y component of vorticity distribution at the moment $\frac{U_0 t}{c} = 30$. The suction surface vorticity is positive, while the lifting surface vorticity is negative. The opposite signs of the vortices on the two surfaces is the cause of the lift generated by the hydrofoil. There is a small amount of negative vorticity on the suction surface. This corresponds to the closure of the cavity, which is also the place where the re-entrant jet appears, so there is a special distribution of quadrupole.

Hydroacoustic analysis

Four integration methods are used to predict the sound pressure for the four acoustic probes in the figure 3, by the integration on the object, the

integration on the penetrable surface (the same position as the volume area), the volume integral, and the volume integral of two-phase flow. The sampling frequency is 5×10^5 Hz, and the sampling duration is 0.6 s.

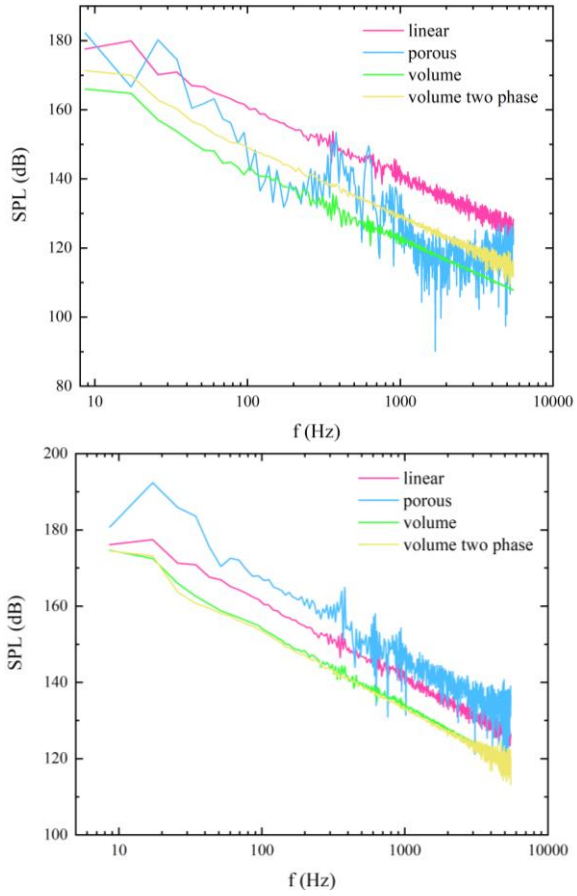

Fig. 8 Sound pressure level (SPL) with four methods at microphones A and B (top panel is for A, and bottom panel is for B).

Here is an introduction on how to consider the volume integral of the two-phase fluid. Based on the formula introduced in Section 2.3, the change of sound wave velocity is considered. When the alpha value is greater than 0.5, the medium in the grid is considered to be water, and the speed of sound is 1400m/s; when the alpha value is less than 0.5, the medium in the grid is considered to be vapor, and the speed of sound is 340m/s.

$$c_{\text{multiphase}} = \begin{cases} 1400, & \alpha > 0.5 \\ 340, & \alpha \leq 0.5 \end{cases} \tag{21}$$

The frequency domain results are obtained by performing the Fast Fourier Transform (FFT) on the time history. Traditionally, the sound pressure level (SPL) are used to express the magnitude of sound pressure. The SPL calculation formula is as follows:

$$\text{SPL} = 20 \times \log_{10}\left(\frac{p}{p_{ref}}\right) \tag{22}$$

The 4 test points can be divided into two categories: upstream probes and downstream microphones for hydrofoil cavitation.

Microphone 'A' is in the initial stage of cavitation, and the nonlinear effect is not obvious. Its linear term (object surface integration) is larger than the nonlinear term (volume integral), which is about 10 dB higher, as figure 8 shows. The contribution of the linear term is close to the nonlinear term at probe 'B'. The role of the nonlinear term becomes more obvious at this time. This is in line with previous studies. The quadrupoles are often produced due to turbulence effects (such as vortex shedding, cavitation, etc.).

As for peak frequency, the results of object surface integration, volume integration, and two-phase volume integration are similar (about 18 Hz), which corresponds to the cavitation development frequency. But the peak frequency of penetrable integral has a large deviation.

Figure 9 shows the SPL of the two downstream probes 'C' and 'D'. As the cavitation gradually disappears, the SPL of the nonlinear term at points 'C' and 'D' decreases compared to points 'A' and 'B'. It is worth noting that at point 'C', there is a clear difference between considering the two-phases volume integration and the direct volume integration, but at point 'D', the two are relatively close. The reason for this difference needs further research.

In terms of peak frequency, the peak frequencies of downstream points C and D are the same as upstream points A and B, because the cycle of cavitation development remains unchanged upstream and downstream.

In order to facilitate the comparison, we compiled the sound pressure level at the peak frequency predicted by the four methods at the 4 sound pressure test points into Table 2. It is used to quantitatively compare the sound pressure prediction results of different methods at different locations for hydrofoil cavitation.

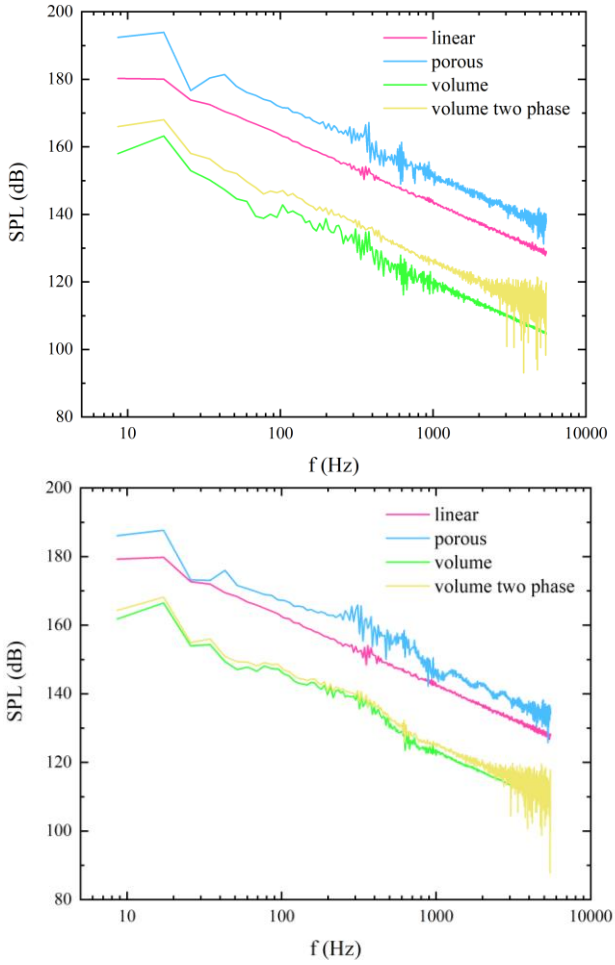

Fig. 9 Sound pressure level (SPL) with four methods at microphones C and D (top panel is for C, and bottom panel is for D).

Table 2. The corresponding sound pressure level (at respective peak frequency) of the frequency domain curve predicted by the 4 methods at the 4 test points.

Method / Position	Linear	Porous	Volume	Two-phase
Microphone 'A'	180.4 dB	180.9 dB	165.5 dB	171.6 dB
Microphone 'B'	177.1 dB	192.3 dB	173.5 dB	173.6 dB
Microphone 'C'	180.3 dB	193.0 dB	161.9 dB	168.7 dB
Microphone 'D'	180.1 dB	188.9 dB	167.8 dB	169.7 dB

At each test point, the peak SPL of the linear component is higher than that of the nonlinear component (volume integration). This does not mean that the linear component is more important than the nonlinear component. In fact, due to the strong effect of the cavitation viscosity, nonlinear effects are considered to be large. The linear component is dominated by the vented vortex, so the energy at the peak is more concentrated. However, the nonlinear component is dispersed in various frequency ranges.

Furthermore, the criterion for the two-phase sound speed used in this paper is $\alpha = 0.5$, but some literatures believe that the threshold of cavitation is 0.9 (Kim et al., 2017). A more accurate consideration should be to obtain the sound speed of each grid by interpolation according to the α value. It needs further research in the future.

CONCLUSIONS

This paper takes two-dimensional NACA66 (MOD) as an example to study the linear sound pressure and nonlinear sound pressure characteristics of hydrofoil cavitation noise. The open source software OpenFOAM is used to simulate the cavitation flow and sound field. The turbulence model is selected as SA-DDES, the cavitation model is the Schnerr-Sauer model. The nonlinear sound pressure signal is calculated by the direct volume integration ignoring the time delay. In addition, a new integration method suitable for volume integral is proposed for the two phase flow. The conclusions are as follow:

- Under low Reynolds number and small angle of attack, the hydrofoil cavitation type is sheet cavitation. At this time, the cavity is generated by the leading edge and attaches to the suction surface of the hydrofoil and hardly changes with time. In the closure area of the cavitation, a re-entrant jet is generated. The vorticity is mainly concentrated in the area of the cavity.

- For the upstream sound pressure of the hydrofoil, the linear term is greater than the nonlinear term. The linear term is similar to the nonlinear term near the closure area of the cavity. The closer the probe is to the downstream of the hydrofoil, the more obvious the peak frequency of the nonlinear term.

- Considering the volume integral of the two phases has a great impact on the results of nonlinear sound pressure prediction, especially near the closure area of the cavity. Therefore, it is necessary to conduct in-depth research on the nonlinear term of cavitation noise in two-phase flow in the future.

ACKNOWLEDGEMENTS

This work was supported by the National Natural Science Foundation of China (51879159, 52131102), and the National Key Research and Development Program of China (2019YFB1704200), to which the authors are most grateful.

REFERENCE

Ahn, B. K., Jeong, S. W., Kim, J. H. (2016). Experimental Investigation of Cavity Patterns and Noise Characteristics. In International Conference on Offshore Mechanics and Arctic Engineering (Vol. 49989, p. V007T06A100). American Society of Mechanical Engineers.

Bensow, R., Liefvendahl, M. (2016). An acoustic analogy and scale-resolving flow simulation methodology for the prediction of propeller radiated noise. In 31th Symposium on Naval Hydrodynamics, California.

Choi, W. S., Choi, Y., Hong, S. Y., Song, J. H., Kwon, H. W., Jung, C. M. (2016). Turbulence-induced noise of a submerged cylinder using a permeable FW–H method. International Journal of Naval Architecture and Ocean Engineering, 8(3), 235-242.

Cianferra, M., Armenio, V., Ianniello, S. (2018). Hydroacoustic noise from different geometries. International Journal of Heat and Fluid Flow, 70, 348-362.

Cianferra, M., Ianniello, S., Armenio, V. (2019). Assessment of methodologies for the solution of the Ffowcs Williams and Hawkings equation using LES of incompressible single-phase flow around a finite-size square cylinder. Journal of Sound and Vibration, 453, 1-24.

Curle, N. (1955). The influence of solid boundaries upon aerodynamic sound. Proceedings of the Royal Society of London. Series A. Mathematical and Physical Sciences, 231(1187), 505-514.

Deane, G. B., Stokes, M. D. (2010). Model calculations of the underwater noise of breaking waves and comparison with experiment. The Journal of the Acoustical Society of America, 127(6), 3394-3410.

Epikhin, A., Evdokimov, I., Kraposhin, M., Kalugin, M., Strijhak, S. (2015). Development of a Dynamic Library for computational aeroacoustics applications using the OpenFOAM Open Source Package. Procedia Computer Science, 66, 150-157.

Ffowcs Williams, J. E., Hawkings, D. L. (1969). Sound generation by turbulence and surfaces in arbitrary motion. Philosophical Transactions of the Royal Society of London. Series A, Mathematical and Physical Sciences, 264(1151), 321-342.

He, X., Liu, Z., Wang, X., & Yuan, Z. (2020). Numerical Prediction of the Hydrofoil Noise. In Journal of Physics: Conference Series (Vol. 1650, No. 3, p. 032027). IOP Publishing.

Ianniello, S., Muscari, R., Di Mascio, A. (2013). Ship underwater noise assessment by the acoustic analogy. Part I: nonlinear analysis of a marine propeller in a uniform flow. Journal of marine Science and technology, 18(4), 547-570.

Kim, S., Cheong, C., Park, W. G. (2017). Numerical investigation on cavitation flow of hydrofoil and its flow noise with emphasis on turbulence models. Aip Advances, 7(6), 065114.

Kim, S., Cheong, C., Park, W. G. (2018). Numerical investigation into effects of viscous flux vectors on hydrofoil cavitation flow and its radiated flow noise. Applied Sciences, 8(2), 289.

Leroux, J. B., Astolfi, J. A., Billard, J. Y. (2004). An experimental study of unsteady partial cavitation. J. Fluids Eng., 126(1), 94-101.

Lighthill, M. J. (1952). On sound generated aerodynamically I. General theory. Proceedings of the Royal Society of London. Series A. Mathematical and Physical Sciences, 211(1107), 564-587.

Marine environment protection committee. (2014). Noise from

Commercial Shipping and its Adverse Impacts on Marine life, in: IMO (Ed.) MEPC 66/17.
Schmalz, J., Kowalczyk, W. (2015). Implementation of acoustic analogies in OpenFOAM for computation of sound fields. Open Journal of Acoustics, 5(02), 29.
Schnerr, G. H., Sauer, J. (2001). Physical and numerical modeling of unsteady cavitation dynamics. In Fourth international conference on multiphase flow (Vol. 1). ICMF New Orleans.
Singhal, A. K., Athavale, M. M., Li, H., Jiang, Y. (2002). Mathematical basis and validation of the full cavitation model. J. Fluids Eng., 124(3), 617-624.
Spalart, P., Allmaras, S. (1992). A one-equation turbulence model for aerodynamic flows. In 30th aerospace sciences meeting and exhibit (p. 439).
Sun, T., Wang, Z., Zou, L., Wang, H. (2020). Numerical investigation of positive effects of ventilated cavitation around a NACA66 hydrofoil. Ocean Engineering, 197, 106831.
Wang, W., Li, Z., Liu, M., Ji, X. (2021). Influence of water injection on broadband noise and hydrodynamic performance for a NACA66 (MOD) hydrofoil under cloud cavitation condition. Applied Ocean Research, 115, 102858.
Wu, Q., Huang, B., Wang, G., Cao, S., Zhu, M. (2018). Numerical modelling of unsteady cavitation and induced noise around a marine propeller. Ocean Engineering, 160, 143-155.
Yu, A., Wang, Y. F., Tang, Q. H., & Zhou, D. Q. (2021). Analysis of dipole noise level characteristics of NACA0015 hydrofoil under different working conditions. Journal of Hydrodynamics, 33(1), 63-73.